J. Fluid Mech. (2009), *vol.* 630, *pp.* 391–411.
doi:10.1017/S002211200900682X Printed in the United Kingdom

Lagrangian drift near a wavy boundary in a viscous oscillating flow

E. LARRIEU[1], E. J. HINCH[2] AND F. CHARRU[1]†

[1]Institut de Mécanique des Fluides de Toulouse, UMR CNRS/INPT/UPS 5502, 2, Avenue Camille Soula, 31400 Toulouse, France

[2]CMS-DAMTP, Wilberforce Road, Cambridge CB3 0WA, UK

(Received 21 August 2008 and in revised form 4 March 2009)

The formation of sand ripples in oscillating flows is thought to be due to a steady streaming current which near the bottom is towards the crests. We present quantitative observations of this mean flow over self-formed and artificial ripples, by observing the displacement of a coloured filament after a number of oscillations in the simple situation of viscous Couette flow. Confusingly, the filament moves in the 'wrong' direction, because it follows the Lagrangian mean flow. We calculate the Lagrangian mean flow. A complication is that the amplitudes of the oscillations in the experiments are not small. We compare the predictions with the experimental observations of displacements of the filament, showing good agreement.

1. Introduction

1.1. *Scope of the paper*

The oscillating motion of a fluid may generate a slow Eulerian mean flow related to inertia effects, known as 'steady streaming' (Riley 2001). Such a mean flow can be produced by acoustic waves in compressible flow (Rayleigh 1883; Lighthill 1978) or surface waves in incompressible irrotational flow (Stokes 1847). It can also arise in incompressible flows oscillating near a solid boundary or in the reverse situation of an oscillating wall in a fluid at rest, whenever there exists a gradient of the wave phase or wave amplitude (Batchelor 1967). A phase gradient typically corresponds to a gravity wave travelling over a flat bottom; here the streaming flow is uniform and consists of a near-bed jet in the direction of the wave advance (Longuet-Higgins 1953; Unluata & Mei 1970; Craik 1982). A gradient of the amplitude is encountered when the fluid oscillates over a wavy wall; there the streaming flow has a cellular structure, spatially periodic.

The latter situation of fluid oscillation over a wavy bottom is of particular importance when the bottom is erodible, typically a sand bed. Over any disturbance of the flat bottom, advection generates a mean flow which is directed from troughs to crests near the bed. When stronger than stabilizing effects such as that of gravity, this flow drags the particles up to the crests, thus amplifying the bottom disturbance. This is the usual explanation of the formation of 'rolling grain ripples' on a sandy bottom, first analysed by Bagnold (1946). However, a quantitative assessment of the relation between the streaming flow and the particle flux is still lacking. In fact, no

† Email address for correspondence: francois.charru@imft.fr

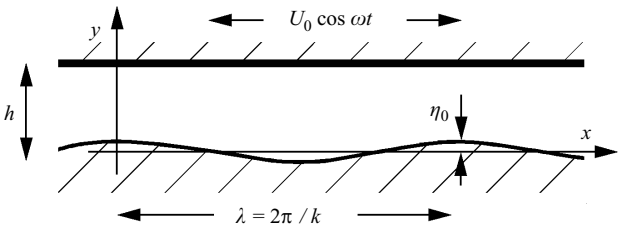

FIGURE 1. Sketch of the oscillating flow over a wavy bottom.

experimental evidence has been provided, until now, that the shear stress associated with the streaming flow over a wavy bottom is responsible for the particle drift.

The present paper reports calculations and measurements of the fluid drift associated with an oscillating Couette flow over a wavy bottom, either fixed or erodible (figure 1). Observations of particle motion will be reported in a future paper. This paper follows previous investigations aiming at a better understanding of the interaction of the fluid flow and particle motion (Charru, Mouilleron-Arnould & Eiff 2004; Charru *et al.* 2007). For practical reasons, these experiments involve a viscous Couette flow with finite depth. This situation does not correspond to that of ripples formed by water, but it allows the desired observations and accurate comparison with theory. Note that viscous flow is also relevant to some engineering applications (Schaflinger, Acrivos & Stibi 1995; Wallner & Schaflinger 1998; Charru & Mouilleron-Arnould 2002). In particular, observations of ripple formation under oscillatory flow in a capillary tube have been reported by Zoueshtiagh *et al.* (2008), in connection with microfluidic issues. In the experiments to be presented, it appeared first that the direction of the observed drift of fluid particles was opposite to the one expected. It was then realized that these observations corresponded to the Lagrangian drift, whereas calculations were for the Eulerian velocity. Hence the Lagrangian drift calculations form the theoretical part of this paper. Flow calculations corresponding to our experiments are presented in §§ 2 and 3, with the solution for small-amplitude oscillations in § 4 and then for large amplitudes in § 5 because the amplitudes in the experiments were not small. The experiments are then presented and measurements compared to the calculations in § 6. Conclusions are given in § 7. The remaining part of this section is devoted to a review of the literature on streaming flow over a wavy bed.

1.2. *Streaming flow over a wavy bed: review of the literature*

We start with a focus on theoretical studies, proceeding to experiments towards the end. The problem is complicated with seven independent length scales, although one is not relevant to flow calculations, and another is always too large to play a role. Roughly in order of increasing size, they are the following:

(i) d the diameter of the particles, which occurs only in the particle transport and not in the flow;

(ii) η_0 the amplitude of the ripples, necessarily $d \ll \eta_0$;

(iii) λ the wavelength of the ripples; vortices are shed if the slope η_0/λ is not small;

(iv) δ the thickness of a Stokes oscillating boundary layer, $\delta = \sqrt{2\nu/\omega}$;

(v) ℓ the excursion of fluid in the oscillating flow far above the ripples, $\ell = U/\omega$;

(vi) h the depth of water;

(vii) L the wavelength of water waves in the case of sea ripples.

Sea ripples have $\lambda, \delta \ll h, L$, so that h and L become irrelevant. In order to make progress, additional limiting cases are considered by different authors. The first

relevant calculation seems to have been made by Schlichting (1932), who studied the case of a thin boundary layer $\delta \ll h$, small slope $\eta_0 \ll \lambda$ and small fluid excursion $\ell \ll \delta$ to obtain a simple expression for the Eulerian steady streaming. Lyne (1971) first reworked Schlichting's result in his Case i and then tackled large fluid excursions $\ell \gg \delta$ in his Case ii in which he needed to make an additional assumption of thin boundary layers $\delta \ll \lambda$. The problem of Case ii then becomes quasi-stationary, permitting the use of Benjamin's (1959) analysis of the critical layers in the flow. (At the time, Benjamin was interested in wind-generated water waves.) Lyne gave expressions for the Eulerian steady streaming, in Case ii an integral requiring numerical evaluation. Independently, Sleath (1974) derived the same results as Lyne, making minor corrections to certain formulae. In Sleath (1976), he went on to calculate numerically the Lagrangian displacements in Case ii. With simple ideas about the movement of the particles, he suggested ripples would be formed with wavelengths similar to the fluid excursion, $\ell/\lambda = O(1)$, with a weak dependence on the boundary-layer thickness, which was confirmed by his experiments. In this paper, only the wavelength of the ripples was observed.

The next calculation was by Kaneko & Honji (1979), who considered small fluid excursions $\ell \ll \delta$ and expanded in the amplitude of the ripples retaining terms to $O((\eta_0/\delta)^7)$. Numerical assistance was required to evaluate the many coefficients in their solution of coupled ordinary differential equations (ODEs). They found the Eulerian steady streaming in several examples, up to $\eta_0/\delta = 0.7$, without vortex shedding. They also took some photos of the flow pattern of the steady streaming, although it is unclear how their technique eliminated the oscillating component. Note that they only observed the pattern of the flow and its direction and that their calculation yielded no simple expression.

The next development comes with Hara & Mei (1990). They again studied two cases: (i) small fluid excursion $\ell \ll \lambda$ but arbitrary slope $\eta_0/\lambda = O(1)$ and (ii) small slope $\eta_0 \ll \lambda$ but arbitrary fluid excursion $\ell/\lambda = O(1)$. The novelty in their calculation of the flow is to have strong steady streaming. This can occur because while the forcing of the mean flow is small it is limited by viscosity which is small compared with inertia which limits the oscillating components. Stuart (1963) and Riley (1965) had developed the ideas required to tackle this strong steady streaming. It is unlikely that this regime occurs in sea conditions. Hara & Mei (1990) needed to evaluate numerically an infinite system of coupled ODEs. In a later paper, Hara, Mei & Shum (1992) extended the results for Case ii by semi-numerically evaluating a series up to $(\eta_0/\lambda)^6$, without vortex shedding. Shum (1995) used a full numerical method for the flow and then could track the Lagrangian displacement of particles. He gave examples of how dye lines which are initially either vertical or horizontal develop in a chaotic manner. He did not however find the mean flow. Particle transport finally arrived in the studies of this group in Mei & Yu (1997).

At the same time as the Hara & Mei (1990) paper, Blondeaux (1990) introduced for the first time a model of particle transport to be solved in parallel with the flow. For the flow, he linearized in small amplitudes $\eta_0 \ll \delta$ but left the boundary-layer thickness and fluid excursion arbitrary, δ/λ and ℓ/δ both $O(1)$. To evaluate the Eulerian steady streaming, a matrix of coefficients has to be solved numerically. (In the light of the work of Hara & Mei (1990), Blondeaux's approach implicitly assumes weak steady streaming, as did Lyne and Sleath, as is appropriate for sea conditions.) His calculation of the flow is nearly identical to that by Vittori (1989). The particle transport equation predicted the onset condition for ripples in a Froude–Reynolds number phase diagram and predicted the wavelengths of the ripples; these predictions

were tested satisfactorily against new experimental data obtained when Sleath visited Genoa. A second paper by Vittori & Blondeaux (1990) made a small finite-amplitude expansion for ripples near onset in the Froude–Reynolds diagram. Later papers by Blondeaux and Vittori considered three-dimensional effects and turbulent flows with direct numerical simulation (DNS), e.g. Scandura (2007). Calculation of the detached flow over steep ripples, such as that considered by Longuet-Higgins (1981), is a different problem which is not reviewed here.

The case of an oscillating Couette flow, which is relevant to the experiments described in this paper, corresponds to $h \ll \delta$, so there is no boundary layer. It is not possible to take a limit of the results above for sea ripples with $\delta \ll h$ to obtain any results for our experiments with $h \ll \delta$. This situation was investigated by Charru & Hinch (2006*b*), who calculated the Eulerian mean flow for long waves of small amplitude ($\eta_0 \ll h \ll \lambda$) and ℓ/λ arbitrary. An erosion–deposition model for the particles was used, first introduced in Charru & Hinch (2006*a*) (see also Charru 2006). However the Lagrangian drift necessary here was not calculated.

Turning to experiments, it appears that these are far fewer than theoretical analyses. Most deal with the steady streaming near a flat bottom induced by propagating surface water waves. Early results are discussed by Longuet-Higgins (1953), while recent measurements are by Ourmières & Mouazé (2007). These results for a flat bed cannot help to understand the formation of ripples.

For oscillating flow over rippled beds, many visualizations can be found in the literature, providing qualitative pictures of instantaneous streamlines with the important vortex behind sharp-crested (large-amplitude) ripples (see e.g. Ourmières & Chaplin 2004). Marin (2004) has reported particle image velocimetry (PIV) measurements of the velocity field induced by surface waves over a rippled bed; however, horizontal and time averaging removes the effect of ripples and retains the effect of the surface wave only. Rousseaux *et al.* (2004) presented PIV measurements above ripples, showing transient eddies in qualitative agreement with the calculations by Vittori (1989), but the mean flow was not measured. The only quantitative measurement of the mean Eulerian flow we found is that of Du Toit & Sleath (1981). Their experiment consists in oscillating a body of water over self-formed ripples, with parameters corresponding to rough turbulent regime (with $\ell/\lambda = 0.74$, $\lambda/\delta = 126$, $2\eta_0/\lambda = 0.20$). Measurements at $\lambda/6$ and $\lambda/3$ from the crest were compared with numerical simulation of the Navier–Stokes equations, showing same flow direction but quantitative differences of the order of the velocity itself.

2. Idealized problem

Motivated by the experiments to be described in § 6, we study a thin layer of viscous liquid driven in a planar Couette flow by a sideways-oscillating top boundary and perturbed by a stationary wavy-bottom boundary of sinusoidal form (figure 1). The Stokes drift and Eulerian mean flow due to small inertial effects are calculated. Two cases are considered: (i) small-amplitude displacements of the top boundary compared to the wavelength of the wavy bottom and (ii) arbitrary amplitudes.

2.1. *Problem statement*

We solve the incompressible Navier–Stokes equations

$$\rho\left(\frac{\partial \boldsymbol{u}}{\partial t} + \boldsymbol{u}\cdot\nabla\boldsymbol{u}\right) = -\nabla p + \mu\nabla^2\boldsymbol{u},$$

$$\nabla\cdot\boldsymbol{u} = 0,$$

subject to no-slip boundary conditions on the top plate which oscillates with frequency ω and velocity amplitude U_0,

$$\boldsymbol{u} = (U_0 \cos \omega t, 0, 0) \quad \text{on } y = h,$$

and on the stationary wavy bottom which has a perturbation amplitude η_0, wavenumber k and sinusoidal form

$$\boldsymbol{u} = 0 \quad \text{on } y = \eta_0 \cos kx.$$

The amplitude of the perturbation is taken to be small compared with the height of the channel, $\eta_0 \ll h$, and also to have small slope, $k\eta_0 \ll 1$.

The Lagrangian motion $\boldsymbol{x}(t)$ is found by integrating the flow

$$\dot{\boldsymbol{x}} = \boldsymbol{u}(\boldsymbol{x}, t).$$

2.2. *Non-dimensionalization*

We scale vertical distances y on the height of the channel h, horizontal distances x on the wavenumber of the wavy bottom k and time t on the frequency ω. Hence the horizontal velocities u are scaled on ω/k and vertical velocities v on ωh.

This non-dimensionalization produces four non-dimensional groups of parameters, three of which we take to be small:

(i) Thin-layer approximation, $kh \ll 1$. We assume that the channel height is small compared with the wavelength. We shall calculate only the leading-order term in this approximation. The corrections are $O((kh)^2)$ and have the same phase as the leading-order term and so produce only small corrections to the mean effects.

(ii) Small-disturbance approximation, $\epsilon = \eta_0/h \ll 1$. We assume that the magnitude of the perturbations of the bottom boundary are small compared with the height of the channel. In the thin-layer approximation, this restriction on the magnitude also makes the slope small. We need to find the $O(1)$ base flow for a flat-bottom boundary and then the first correction $O(\epsilon)$ due to the wavy bottom.

(iii) Small Reynolds number $Re = \rho\omega h^2/\mu \ll 1$. We assume that inertial effects measured by an oscillating Reynolds number are small. The leading-order $O(1)$ terms are a Stokes flow which is reversible and so produces no mean Eulerian flow and no mean Stokes drift. Hence we need to consider the small first corrections $O(Re)$. (Note that the classical Reynolds number $\rho U_0 h/\mu$ is the combination ReA/kh, where A is defined below.)

(iv) Amplitude $A = kU_0/\omega$. The fourth non-dimensional group is the ratio of the displacement of the oscillating top plate to the wavelength of the wavy bottom, kU_0/ω. We shall first consider the case of small displacements $A \ll 1$ and then order-one displacements $A = O(1)$.

2.3. *Non-dimensionalized problem*

In the thin-layer approximation, we need only solve the horizontal momentum equation

$$Re\left(\frac{\partial u}{\partial t} + u\frac{\partial u}{\partial x} + v\frac{\partial u}{\partial y}\right) = -\frac{\partial p}{\partial x} + \frac{\partial^2 u}{\partial y^2}.$$

Here we have omitted the $O((kh)^2)$ small horizontal diffusion of momentum. To leading order with an $O((kh)^2)$ correction, the vertical component of the momentum equations gives that the horizontal pressure gradient does not depend on vertical position; i.e. it is only a function of horizontal position and time. The vertical

component of velocity is instead found from the incompressibility

$$\frac{\partial u}{\partial x} + \frac{\partial v}{\partial y} = 0.$$

Integrating this condition from the lower boundary, which to the approximations we consider may be taken to be the unperturbed lower boundary $y = 0$, to the upper boundary gives the constraint that the horizontal flux

$$\int_0^1 u \, \mathrm{d}y \quad \text{is independent of } x.$$

This constraint determines at each x the horizontal pressure gradient.

The non-dimensionalized boundary conditions are

$$\boldsymbol{u} = (A\cos t, 0) \quad \text{on } y = 1,$$
$$\boldsymbol{u} = 0 \quad \text{on } y = \epsilon \cos x.$$

And finally the Lagrangian motion is calculated from

$$\dot{\boldsymbol{x}} = \boldsymbol{u}(\boldsymbol{x}, t).$$

2.4. *Expansion*

We make a double expansion in the two small parameters of the small disturbance ϵ and small inertial effects Re:

$$u \sim \overline{u}^0 + Re\overline{u}^i + \epsilon(\tilde{u}^0 + Re\tilde{u}^i),$$
$$v \sim \epsilon(\tilde{v}^0 + Re\tilde{v}^i),$$
$$p \sim \epsilon(\tilde{p}^0 + Re\tilde{p}^i).$$

The superscript 0 denotes the leading-order Stokes flow, while the superscript i denotes the first corrections due to inertia. The overbars denote the solution for a flat bottom, while the tildes denote the first disturbances produced by the wavy bottom. For the flat bottom there is no vertical flow and no pressure gradient.

Substituting the expansion into the boundary conditions yields on the top boundary

$$\overline{u}^0 = A\cos t \quad \text{on } y = 1,$$

with all other horizontal and vertical velocity components in the above expansion vanishing on the top boundary. Transferring the boundary condition from $y = \epsilon \cos x$ to the mean position $y = 0$, we have

$$\tilde{u}^0 + \frac{\partial \overline{u}^0}{\partial y}\cos x = 0 \quad \text{and} \quad \tilde{u}^i + \frac{\partial \overline{u}^i}{\partial y}\cos x = 0 \quad \text{on } y = 0,$$

with all the other velocity components in the expansion above vanishing on $y = 0$.

3. Solution for flow

3.1. *Couette flow*

The base flow is the Couette flow for a flat bottom,

$$\overline{u}^0 = \overline{U}^0(y)\cos t \quad \text{with } \overline{U}^0 = Ay.$$

3.2. *Inertial correction*

The inertial correction $\overline{u}^i$ is governed by

$$\frac{\partial^2 \overline{u}^i}{\partial y^2} = \frac{\partial \overline{u}^0}{\partial t},$$

subject to boundary conditions of vanishing on $y = 0$ and 1. The solution is

$$\overline{u}^i = \overline{U}^i(y) \sin t \quad \text{with } \overline{U}^i = \tfrac{1}{6} A(y - y^3).$$

While the base Couette flow moves to the right at $t = 0$, inertia makes the flow continue flowing to the right at $t = \pi/2$, at which time the top plate is stationary.

3.3. *Stokes perturbation due to wavy bottom*

The first correction due to the wavy bottom $\tilde{u}^0$ is governed by

$$0 = -\frac{\partial \tilde{p}^0}{\partial x} + \frac{\partial^2 \tilde{u}^0}{\partial y^2},$$

subject to

$$\tilde{u}^0 = \begin{cases} 0 & \text{on } y = 1, \\ -A \cos x \cos t & \text{on } y = 0, \end{cases}$$

with the pressure gradient $\partial \tilde{p}^0 / \partial x$ such that there is no mean flux $\int \tilde{u}^0 \, \mathrm{d}y$ varying with $\cos x$. The solution is

$$\tilde{u}^0 = \tilde{U}^0(y) \cos x \cos t \quad \text{with} \quad \tilde{U}^0 = A(-1 + 4y - 3y^2).$$

At low levels near the crest of the wavy bottom $x = 0$, this horizontal velocity is negative when the base flow is positive, in order for the sum of these flows to vanish on the crest. At higher levels the flow is positive over the crests, because there is no net horizontal flux.

Using the incompressibility condition, the vertical component of velocity can be found,

$$\tilde{v}^0 = \tilde{V}^0(y) \sin x \cos t \quad \text{with } \tilde{V}^0 = A(-y + 2y^2 - y^3).$$

This flow is downwards between the crest at $x = 0$ and trough at $x = \pi$ at times when the base flow is positive.

3.4. *Inertial correction to wavy-bottom disturbance*

The inertial correction $\tilde{u}^i$ to the above disturbance is governed by

$$-\frac{\partial \tilde{p}^i}{\partial x} + \frac{\partial^2 \tilde{u}^i}{\partial y^2} = \frac{\partial \tilde{u}^0}{\partial t} + \overline{u}^0 \frac{\partial \tilde{u}^0}{\partial x} + \tilde{v}^0 \frac{\partial \overline{u}^0}{\partial y},$$

subject to

$$\tilde{u}^i = \begin{cases} 0 & \text{on } y = 1, \\ -\frac{1}{6} A \cos x \sin t & \text{on } y = 0, \end{cases}$$

with the pressure gradient $\partial \tilde{p}^i / \partial x$ such that there is no mean flux $\int \tilde{u}^i \, \mathrm{d}y$ varying with $\cos x$ and $\sin x$. The solution is

$$\tilde{u}^i = \tilde{U}^{i1}(y) \cos x \sin t + \tilde{U}^{i2}(y) \sin x \cos^2 t,$$

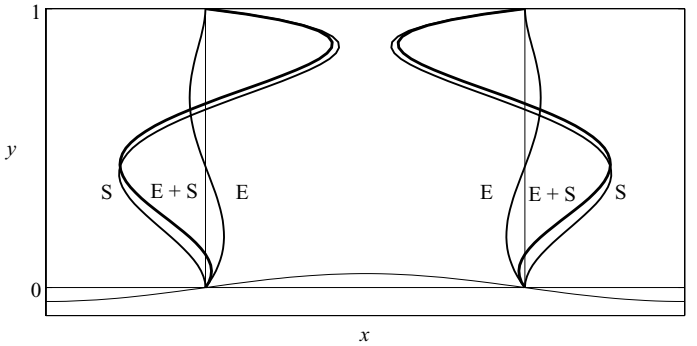

FIGURE 2. The Eulerian mean (E; (3.1)), Stokes drift (S; (4.1)) and Lagrangian mean horizontal velocity (E + S) divided by $A^2\epsilon Re$ as a function of height across the channel Y, on the up and down slopes.

with

$$\tilde{U}^{i1} = \tfrac{1}{60}A(-10 + 32y + 3y^2 - 40y^3 + 15y^4),$$
$$\tilde{U}^{i2} = \tfrac{1}{60}A^2(-2y + 6y^2 - 10y^4 + 6y^5).$$

At time $t = \pi/2$, the contribution from $\tilde{U}^{i1}$ to the flow is negative at low levels over the crest $x = 0$ and positive at high levels, with no net flux. It has two parts, one from inertia making the flow $\tilde{u}^0$ continue in time an extra $\pi/2$ and one from the boundary condition where a negative value is needed on the crests when the flow $\overline{u}^i$ is positive (at $t = \pi/2$). The contribution to the flow from $\tilde{U}^{i2}$ is towards the crests at low levels, away from the crests above, and vanishes on both boundaries. It is driven by advection by the base flow $\overline{u}^0$ of the vorticity associated with $\tilde{u}^0$. There is a positive advection of negative vorticity from the crest at $x = 0$ towards $x = \pi/2$ at $t = 0$ and at $t = \pi$ a negative advection of negative vorticity towards $x = \pi/2$ from the trough at $x = \pi$. Both advections result in negative vorticity being deposited at $x = \pi/2$, which produces there a negative flow at low levels and a positive velocity above.

The $\tilde{U}^{i2}$ part has the Eulerian mean flow,

$$\langle u(x, t)\rangle = \epsilon Re\tfrac{1}{2}\tilde{U}^{i2}(y)\sin x, \tag{3.1}$$

which at low levels is towards the crests, i.e. negative at $x = \pi/2$ and positive at $x = -\pi/2$ (see figure 2).

Using the incompressibility condition, the vertical component of velocity can be found,

$$\tilde{v}^i = \tilde{V}^{i1}(y)\sin x \sin t + \tilde{V}^{i2}(y)\cos x \cos^2 t,$$

with

$$\tilde{V}^{i1} = \tfrac{1}{60}A(-10y + 16y^2 + y^3 - 10y^4 + 3y^5),$$
$$\tilde{V}^{i2} = \tfrac{1}{60}A^2(y^2 - 2y^3 + 2y^5 - y^6).$$

At $t = \pi/2$, the contribution to the flow from $\tilde{V}^{i1}$ is positive at $x = -\pi/2$ before the crest and is negative at $x = \pi/2$ after the crest, giving the return flow of $\tilde{U}^{i1}$ which on the crest is negative a low levels and positive above. The contribution to the flow from $\tilde{V}^{i2}$ is positive over the crests, giving the return flow of $\tilde{U}^{i2}$ which is towards the crests at low levels.

4. Stokes drift at small amplitude, $A \ll 1$

We first make the classical calculation of Stokes drift, assuming that a Lagrangian particle moves only a small distance from its central position $\boldsymbol{X}$ during a single oscillation; i.e. we write

$$\boldsymbol{x}(t) \sim \boldsymbol{X}(T) + \boldsymbol{\delta x}(t),$$

with the horizontal displacement small compared with the wavelength and the vertical displacement small compared with the height, $|\boldsymbol{\delta x}| \ll 1$ in our nondimensionalization. These restrictions are achieved if the amplitude of the oscillation of the top plate is small, $A \ll 1$. The central position $\boldsymbol{X}$ changes very little during one oscillation, drifting as we shall find later on the long time scale of $1/\epsilon Re$, so we set $T = \epsilon Ret$. To leading order, the small displacements are simply integrals in time of the above velocity components evaluated at a fixed position $\boldsymbol{X}$, i.e.

$$\dot{\boldsymbol{\delta x}} = \boldsymbol{u}(\boldsymbol{X}, t),$$

where we need only include the oscillatory components of the flow.

The Lagrangian mean motion of a fluid particle comes partly from the Eulerian mean motion at a fixed point, $\langle \boldsymbol{u}(\boldsymbol{X}, t) \rangle$ averaging in time, together with the Stokes drift which comes from the correction to the calculation above when the flow is evaluated at the slightly displaced position $\boldsymbol{X} + \boldsymbol{\delta x}$ instead of at $\boldsymbol{X}$. Thus the Stokes drift is classically calculated as

$$\boldsymbol{V}_{Stokes} = \langle \boldsymbol{\delta x} \cdot \nabla \boldsymbol{u}|_X \rangle,$$

again averaging over time.

4.1. *Linear displacements*

Making again the double expansion in the two small parameters ϵ and Re

$$\begin{aligned} \delta x &\sim \overline{x}^0 + Re\overline{x}^i + \epsilon(\tilde{x}^0 + Re\tilde{x}^i), \\ \delta y &\sim \epsilon(\tilde{y}^0 + Re\tilde{y}^i), \end{aligned}$$

we find by simple integration in time

$$\begin{aligned} \overline{x}^0 &= \overline{U}^0(Y)\sin t, \\ \overline{x}^i &= -\overline{U}^i(Y)\cos t, \\ \tilde{x}^0 &= \tilde{U}^0(Y)\cos X \sin t, \\ \tilde{y}^0 &= \tilde{V}^0(Y)\sin X \sin t, \\ \tilde{x}^i &= -\tilde{U}^{i1}(Y)\cos X \cos t + \tfrac{1}{4}\tilde{U}^{i2}(Y)\sin X \sin 2t, \\ \tilde{y}^i &= -\tilde{V}^{i1}(Y)\sin X \cos t + \tfrac{1}{4}\tilde{V}^{i2}(Y)\cos X \sin 2t. \end{aligned}$$

In the last two expressions, a drift linear in time has been omitted because it is the Eulerian mean flow.

4.2. *Drift*

We are interested in the x-component of the Stokes drift

$$V_{Stokes} = \left\langle \delta x \frac{\partial u}{\partial x} + \delta y \frac{\partial u}{\partial y} \right\rangle.$$

Now $\overline{u}^0$ and $\overline{u}^i$ are independent of x, so only $\tilde{u}^0$ and $\tilde{u}^i$ contribute to $\partial u/\partial x$. Similarly, δy only has components $\tilde{y}^0$ and $\tilde{y}^i$. Hence the leading contributions to V_{Stokes} are $O(\epsilon)$

and $O(\epsilon Re)$. The $O(\epsilon)$ terms are however products of $\sin t$ and $\cos t$ and so have zero average in time. Hence the leading non-zero mean contributions are $O(\epsilon Re)$, the slow drift rate declared earlier. Thus

$$V_{Stokes} = \epsilon Re \left\langle \overline{x}^0 \frac{\partial \tilde{u}^i}{\partial x} + \overline{x}^i \frac{\partial \tilde{u}^0}{\partial x} + \tilde{y}^0 \frac{\partial \overline{u}^i}{\partial y} + \tilde{y}^i \frac{\partial \overline{u}^0}{\partial y} \right\rangle.$$

Substituting the small displacements and velocity components, we find

$$V_{Stokes} = \frac{1}{2}\epsilon Re \left[-\overline{U}^0 \tilde{U}^{i1} + \overline{U}^i \tilde{U}^0 + \tilde{V}^0 \frac{\mathrm{d}\overline{U}^i}{\mathrm{d}Y} - \tilde{V}^{i1} \frac{\mathrm{d}\overline{U}^0}{\mathrm{d}Y} \right] \sin X.$$

Now substituting the detailed expressions, we obtain

$$V_{Stokes} = \frac{1}{60}\epsilon Re A^2 (6Y^2 - 2Y^3 - 25Y^4 + 21Y^5) \sin X. \tag{4.1}$$

In figure 2 we plot the velocity profiles for this Stokes drift and the Eulerian mean flow obtained earlier, together with their sum, the Lagrangian mean flow. The Stokes drift is away from the crests at low levels and towards the crests at high levels, i.e. in the opposite sense to the Eulerian mean flow. We see that the Stokes drift is about four times larger than the Eulerian mean flow and so dominates the Eulerian mean except very near the bottom boundary, where the Stokes drift vanishes quadratically and the Eulerian mean vanishes linearly. Thus the Lagrangian mean flow is towards the crests in $0 < y < 0.1194$ next to the bottom boundary.

To understand the Stokes drift, consider a particle which starts near to the top boundary in the middle section of the down slope at $x = \pi/2$. Near the top boundary, the wavy bottom causes a slightly stronger oscillation in the narrow section at the crests compared with the wider section at the troughs, with an inertially driven continuation of the oscillation after the top boundary has stopped at $t = \pi/2$. During the first quarter-period, the base flow will move the particle towards the trough where the oscillation is weaker, so the inertially driven continuation is weaker away from the crests, which is equivalent to a small displacement towards the crest. During the next half-period, the base flow moves the particle towards the crest where the oscillation is stronger, so that the inertially driven continuation is stronger towards the crests, which is equivalent to a small displacement also towards the crest. Hence near the top boundary there is a Stokes drift towards the crests. A similar argument can be made to understand the origin of the Stokes drift away from the crests near the bottom boundary. The argument near the bottom boundary is however complicated by the need to include the vertical flow, which near the top vanishes quadratically and so can be ignored there.

Integrating through the depth of the channel, there is no net flux in either the Stokes drift or the Eulerian mean flow. The net Eulerian flux is controlled by the mean pressure gradient, which we have chosen to vanish. The vanishing of the net Lagrangian flux follows from the symmetry of the oscillation.

5. Stokes drift at $A = O(1)$ amplitudes

When the amplitude of the oscillation of the top plate is comparable with the wavelength of the wavy bottom, it is no longer appropriate to consider a Lagrangian fluid particle as moving only a small distance from its central position during a single oscillation. Instead we have to study small deviations relative to an $O(1)$ oscillation

with the base Couette flow, i.e.

$$x(t) \sim \overline{x}^0 + Re\overline{x}^i + \epsilon\tilde{x}^0 + \epsilon Re\tilde{x}^i,$$
$$y(t) \sim \overline{y}^0 + \epsilon\tilde{y}^0 + \epsilon Re\tilde{y}^i,$$

where the oscillation with the base Couette flow is

$$\overline{x}^0 = X(T) + \overline{U}^0(Y)\sin t,$$
$$\overline{y}^0 = Y(T).$$

The drift time remains $T = \epsilon Ret$.

The different order contributions to the displacement must be found from the appropriate contributions to the velocity plus corrections to previous orders of the velocity due to the small displacements. This approach is the required generalization of the standard Stokes drift calculation.

5.1. *Inertial correction to Couette flow*

When the bottom is flat, the flow is horizontal and depends only on the vertical coordinate and time. Thus any correction $Re\overline{x}^i$ to the basic oscillating position $\overline{x}^0$ will not change the value of the $O(Re)$ correction to the flow seen by the moving particle. Hence

$$\dot{\overline{x}}^i = \overline{u}^i = \overline{U}^i(Y)\sin t.$$

And so integrating,

$$\overline{x}^i = -\overline{U}^i(Y)\cos t.$$

5.2. *Wavy-bottom correction to the Stokes flow*

The vertical $O(\epsilon)$ correction to the basic oscillating position changes the $O(\epsilon)$ horizontal velocity seen by the moving particle, although not the vertical velocity,

$$\dot{\tilde{x}}^0 = \tilde{u}^0 + \tilde{y}^0\frac{\mathrm{d}\overline{u}^0}{\mathrm{d}y},$$
$$\dot{\tilde{y}}^0 = \tilde{v}^0.$$

First we tackle the vertical motion,

$$\dot{\tilde{y}}^0 = \tilde{V}^0(Y)\sin[X + \overline{U}^0(Y)\sin t]\cos t,$$

which can be integrated to

$$\tilde{y}^0 = -\tilde{V}^0(Y)\frac{\cos[X + \overline{U}^0(Y)\sin t]}{\overline{U}^0(Y)}.$$

This result can be substituted into the problem for the horizontal motion,

$$\dot{\tilde{x}}^0 = \tilde{U}^0(Y)\cos[\overline{x}^0(t)]\cos t - \tilde{V}^0(Y)\frac{\cos[\overline{x}^0(t)]}{\overline{U}^0(Y)}\frac{\mathrm{d}\overline{U}^0}{\mathrm{d}Y}\cos t,$$

where $\overline{x}^0 = X + \overline{U}^0(Y)\sin t$ is the basic oscillation with the Couette flow. Integrating, we find

$$\tilde{x}^0 = \left[1 - \frac{\tilde{V}^0}{\overline{U}^{0^2}}\right]\frac{\mathrm{d}\overline{U}^0}{\mathrm{d}Y}(\sin[X + \overline{U}^0(Y)\sin t] - \sin X).$$

The last $\sin X$ is a constant of integration, chosen to avoid any singular behaviour as $Y \to 0$. Note that this horizontal displacement has no mean drift, because this approximation is for reversible Stokes flow over a wavy bottom.

5.3. *Inertial correction to wavy-bottom flow*

There are a number of contributions to the $O(\epsilon Re)$ velocity seen by the moving particle.

$$\dot{\tilde{x}}^i = \tilde{u}^i + \tilde{y}^i \frac{\partial \overline{u}^0}{\partial y} + \tilde{y}^0 \frac{\partial \overline{u}^i}{\partial y} + \overline{x}^i \frac{\partial \tilde{u}^0}{\partial x},$$

$$\dot{\tilde{y}}^i = \tilde{v}^i + \overline{x}^i \frac{\partial \tilde{v}^0}{\partial x}.$$

First we tackle the vertical motion:

$$\dot{\tilde{y}}^i = \tilde{V}^{i1}(Y)\sin[\overline{x}^0(t)]\sin t + [\tilde{V}^{i2}(Y) - \overline{U}^i(Y)\tilde{V}^0(Y)]\cos[\overline{x}^0(t)]\cos^2 t,$$

with integral

$$\tilde{y}^i = \int_0^t \tilde{V}^{i1}(Y)\sin[\overline{x}^0(t')]\sin t' + [\tilde{V}^{i2}(Y) - \overline{U}^i(Y)\tilde{V}^0(Y)]\cos[\overline{x}^0(t')]\cos^2 t'\,\mathrm{d}t'.$$

We now find the average in time of the horizontal motion,

$$V_{Lagrangian} = \epsilon Re \left\langle \dot{\tilde{x}}^i \right\rangle.$$

We need several averages of trigonometric functions which can be related to the zeroth Bessel function

$$J_0(z) = \langle \cos(z\sin\theta) \rangle.$$

In particular, we need

$$\langle \sin(z\sin\theta)\sin\theta \rangle = -J_0',$$

$$\langle \cos(z\sin\theta)\cos^2\theta \rangle = J_0 + J_0''$$

$$\text{and} \quad \langle \sin(z\sin\theta)\sin\theta\cos^2\theta \rangle = -J_0' - J_0'''.$$

We then find the Lagrangian mean horizontal velocity as

$$V_{Lagrangian} = \epsilon Re \left[\tilde{U}^{i1} J_0' + \tilde{U}^{i2}(J_0 + J_0'') + \frac{\mathrm{d}\overline{U}^0}{\mathrm{d}Y}(\tilde{V}^{i1} J_0'' - (\tilde{V}^{i2} - \overline{U}^i \tilde{V}^0)(J_0' + J_0''')) \right.$$

$$\left. - \frac{\tilde{V}^0}{\overline{U}^0}\frac{\mathrm{d}\overline{U}^i}{\mathrm{d}Y} J_0' + \overline{U}^i \tilde{U}^0 (J_0 + J_0'') \right] \sin X, \quad (5.1)$$

where all the Bessel functions are evaluated at $z = \overline{U}^0(Y)$. This expression agrees with the Lagrangian mean horizontal velocity found earlier in the limit $A \ll 1$. We can identify $\tilde{U}^{i2}$ in the second term as the Eulerian mean flow. However the large-amplitude oscillation reduces the contribution by a factor $2(J_0 + J_0'')$, by averaging the $\sin x$ in the Eulerian mean over the excursions of the large-amplitude oscillation. At small amplitudes of the displacement of the top boundary, $A \ll 1$, the Lagrangian mean flow increases quadratically, $O(A^2)$. But at very large amplitudes, the Lagrangian mean decreases through the Bessel functions as $O(A^{-1/2})$, due to averaging $\sin x$ over many wavelengths. However near the bottom, there is always a region in which the local amplitude AY is small and in which the small-amplitude predictions are sufficient. In figure 3, we plot the profile of the Lagrangian mean flow divided by

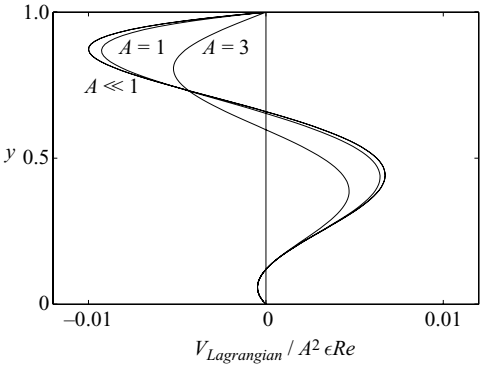

FIGURE 3. The Lagrangian mean horizontal velocity on the down slope at $x = \pi/2$, divided by $A^2\epsilon Re$ as a function of height across the channel Y for $A \ll 1$ ((3.1) and (4.1)), $A = 1$ and $A = 3$ (5.1).

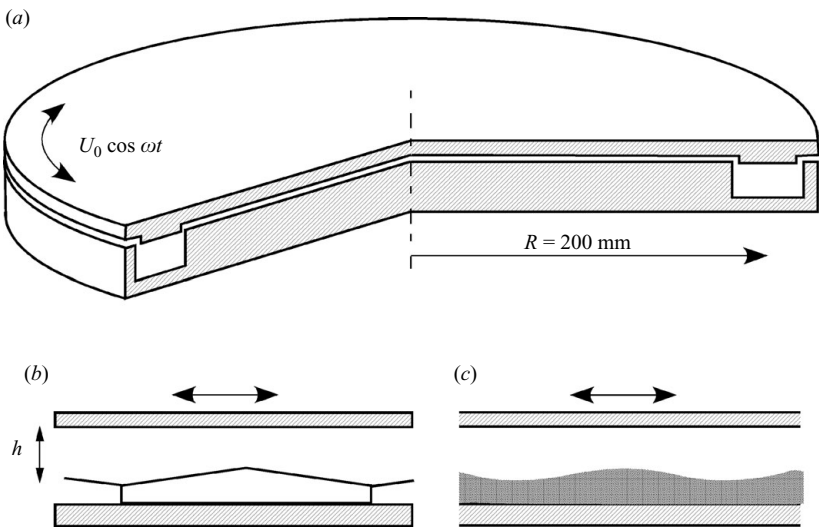

FIGURE 4. Sketch of the annular channel: (*a*) general view with the oscillating upper plate; (*b*) lower wall covered with solid triangular ripples; (*c*) lower wall covered with particles.

$A^2\epsilon Re$ for $A \ll 1$, $A = 1$ and $A = 3$. We see the Lagrangian mean flow does not increase as A^2 for $A > 1$, dropping by 30 % at $A = 3$. We also see that the curves merge near the bottom.

6. Experiments

6.1. *Annular channel*

Experiments were performed in two apparatus, first an annular channel and then a straight channel. The annular channel avoided open-end effects but suffered a small secondary circulation, while the straight channel allowed plane flow but had a gradual loss of particles from the test section and a possible problem of balancing flows.

The annular channel was made of Plexiglas, with mean radius $R = 200$ mm, width $\Delta R = 40$ mm and height $h = 16$ mm (figure 4*a*). The oscillating fluid motion was

created by the rotation of the upper plate, with velocity $U_0 \cos \omega t$. The bottom of the channel was covered with either solid ripples of triangular shape (figure 4*b*) or an erodible bed of particles (figure 4*c*). The wavelength and amplitude of the solid ripples were $2\pi/k = 50\,\text{mm}$ and $\eta_0 = 1\,\text{mm}$ (half vertical distance between troughs and crests), whereas those of the erodible bed were $2\pi/k \approx 70\,\text{mm}$ and $\eta_0 \approx 1\,\text{mm}$. The mean fluid thickness was $h = 15\,\text{mm}$ with the solid bottom and $h = 7\,\text{mm}$ with the erodible bed. PIV and laser Doppler anemometry (LDA) measurements over the flat bottom have shown that the flow is close to plane Couette flow with a small secondary flow directed outwards in the upper half and inwards in the lower half. This secondary flow due to centrifugal forces has characteristic radial velocity $(\rho U_0 h/\mu)\,(h/R)\,U_0$, which is a few percent of U_0 (see Charru *et al.* 2004 for a more complete description).

Two silicone oils with different viscosity were used, $\mu = 0.05\,\text{Pa s}$ (density $\rho = 940\,\text{kg m}^{-3}$) and $\mu = 1\,\text{Pa s}$ ($\rho = 980\,\text{kg m}^{-3}$). The erodible bed was made of acrylic particles with density $\rho_p = 1180\,\text{kg m}^{-3}$; these particles were sieved, and diameter distributions were then determined from optical measurements under a microscope. Two distributions were used, one with mean diameter $d = 0.580\,\text{mm}$ and small standard deviation of 0.044 mm and the other with $d = 0.500\,\text{mm}$ and larger standard deviation of 0.120 mm.

6.2. *Drift over the wavy bottom*

Due to the slowness of the drift motion as compared to that of the main oscillation, techniques providing the instantaneous velocity such as PIV and LDA lack the precision required. The drift has therefore been measured by means of a dyed filament placed vertically in the channel. The dye was first dissolved in a few drops of a mineral oil (Soltrol) and then mixed with the same silicone oil as the surrounding fluid. It was deposited carefully through a small hole in the upper moving plate, with the help of a syringe fitted with a hollow needle. Figure 5(*a*) shows an example of such a filament, enhanced by image processing. Taking care of the verticality of the filament, and of the absence of any bubble or dust, the deformation was reproducible. The motion of the filament was recorded with an interlaced colour CCD camera, with resolution 768×576 pixels and a sampling frequency of 25 Hz. The field of view was $40 \times 30\,\text{mm}^2$. For each run, a few tens of oscillations were recorded. At longer times, molecular diffusion tended to blur the filament, especially for large-amplitude motions or with the low-viscosity fluid. On erodible beds, measurements of the bed profile with an ultrasonic probe (Charru *et al.* 2004) gave the amplitude η_0 and wavelength $2\pi/k$ of the ripple.

As the driving plate was set in oscillatory motion, the filament was stretched back and forth, as shown in figure 5(*a–e*); here the filament was placed above a solid ripple at the middle of a down slope, and the upper plate motion corresponded to dimensionless velocity $A \cos \omega t$ (with scale ω/k). It can be noted that after one period, the filament does not recover its initial straight shape but appears bent (figure 5*e*). This departure from the vertical initial position does not correspond to any drift but to an inertial transient effect due to the fact that the fluid is initially at rest. We have verified that the same departure also occurs over a flat bottom and reaches a stationary shape typically after one period. The displacement of fluid particles corresponding to the exponentially decaying part of the fluid motion, $u^t(y, t)$, can be calculated using the Laplace transform, giving

$$x^t = \int_0^\infty u^t \,\mathrm{d}t = -\frac{A}{6}\,(y - y^3).$$

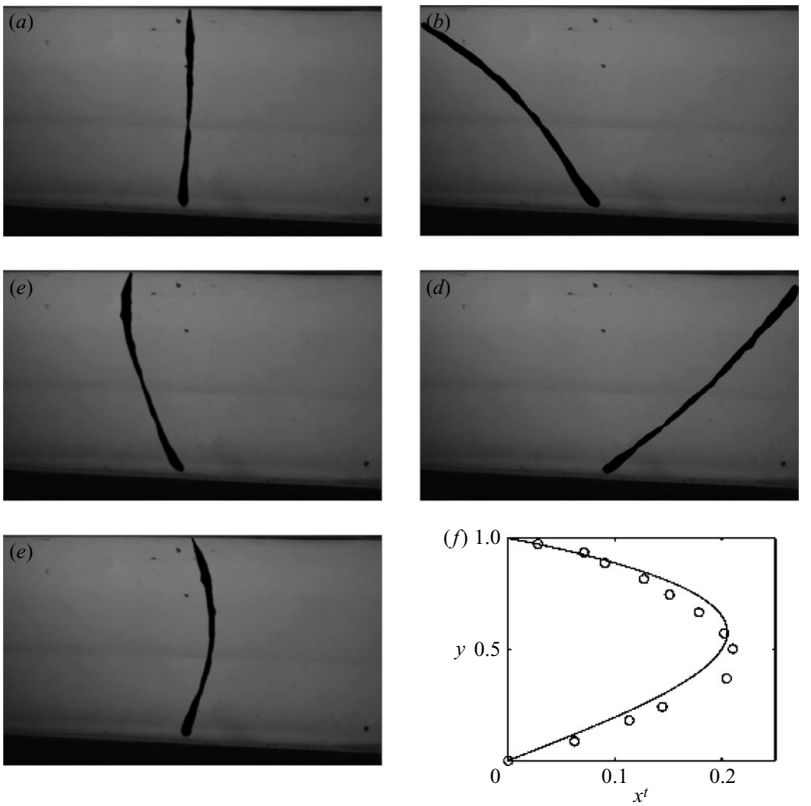

FIGURE 5. Pictures of the dyed filament in the annular channel on the down slope (*a–e*) during the first period at times $25\,\omega t/2\pi = 0$, 2, 12, 23, 25 (with the filament enhanced by image processing) and (*f*) comparison of the dimensionless displacement (○) in (*e*) to the calculation of the transient effect. Parameters: $h = 0.015$ m, $\mu = 1$ Pa s, $U_0 = 0.16$ m s^{-1} and $f = 1$ Hz ($k\eta_0 = 0.126$, $\epsilon = 0.067$, $Re = 1.4$ and $A = 3.2$).

This dimensionless displacement does not depend on the Reynolds number, unlike the characteristic time Re/π^2 of the transient, which was less than unity in the experiments presented here. The displacement after one period shown in figure 5(*e*) is compared to the above prediction in figure 5(*f*), showing good agreement.

As the number of oscillations increases, the drift becomes apparent: the filament at the end of each oscillation takes an S shape whose amplitude increases with time, as illustrated in figure 6(*b*). This figure corresponds to the flow over a solid ripple in the annular channel after 39 oscillations. It can be seen that the drift is directed towards the crest in the upper part of the fluid layer and towards the trough at mid-height, in agreement with the Lagrangian calculations. At a distance of about 1 mm above the bottom boundary, which is about one tenth of the channel height, the displacement is small and the filament nearly vertical. There, close inspection shows that the small drift is directed towards the crest.

We have verified that the deformation is symmetric on the other side of the ripple and that the filament remains straight when it is deposited above a crest or a trough, when the transient effect is subtracted. For other runs with different oscillation frequency and amplitude, and also with the erodible bed, the deformed filament exhibited the same shape.

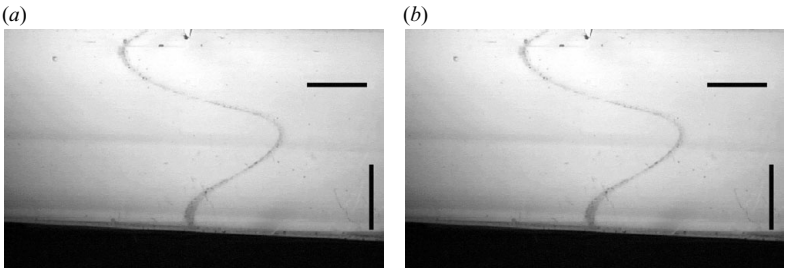

FIGURE 6. Dyed filament in the annular channel, on the right side of a solid ripple: (*a*) initial straight filament; (*b*) deformed filament after 39 periods of oscillation; the length of the dark marks is 5 mm. Same parameters as in figure 5.

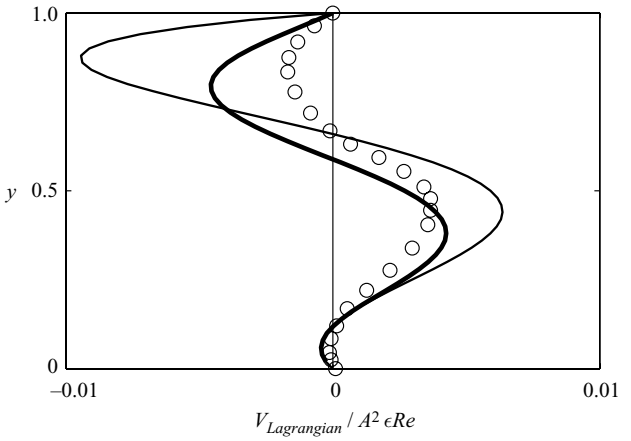

FIGURE 7. Observed drift of the dyed filament in the annular channel (○) compared to the calculations for $A \ll 1$ (thin curve) and $A = 3.2$ (thick curve). Same parameters as in figure 5.

In order to compare quantitatively the measured drift to calculations, points of the deformed filament were extracted from the images. The displacement after one period, which corresponds to the transient effect, was then subtracted from the displacement after typically 40 periods and divided by this time, giving the experimental mean drift velocity. The result is shown in figure 7 and compared to the calculations. It can be seen that in the lower part of the channel, the agreement is good for both the small- and large-amplitude calculations. Near the top moving wall, the velocity from the small-amplitude calculation (thin curve) overpredicts the measured velocity by a factor about 4; the large-amplitude calculation (thick curve) is much closer to measurements. The remaining difference might be due to the Reynolds number being not small as assumed in the calculations ($Re = 1.4$) or to some coupling of the drift and the centrifugal recirculation flow.

6.3. *Further experiments in a straight channel*

The dyed filament in the annular channel was observed to deform radially when seen from above, due to the centrifugal recirculation flow, with displacements in the azimuthal and radial planes of the same order of magnitude. Although the streaming flow due to ripples in the annular channel was *a priori* weakly coupled with the

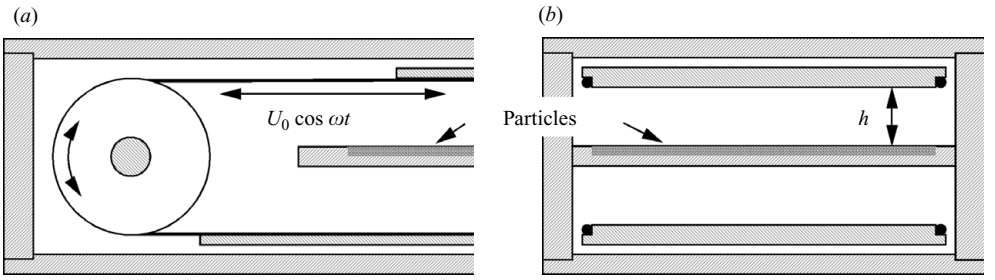

FIGURE 8. Sketch of the straight channel: (*a*) side view showing the pulley driving the oscillating upper and lower plates and the fixed plate supporting the particles; (*b*) cross-view.

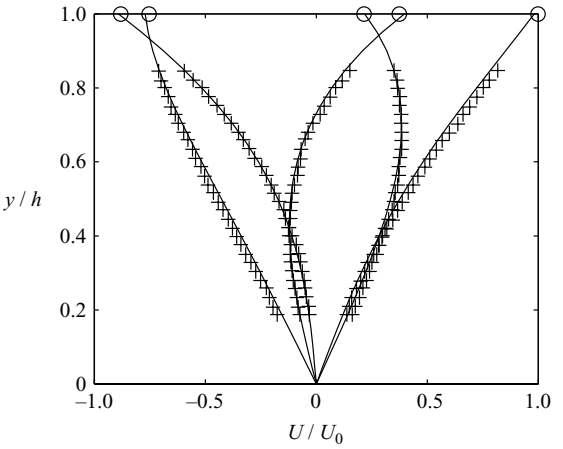

FIGURE 9. Oscillating Couette flow on the flat bottom in the straight channel: (+), measured fluid velocity at the centre of the channel, at phases separated by $2\pi/5$; (○), measured upper plate velocity; (—), solution of the momentum equation at the same phases. Parameters: $f = 0.1$ Hz, $U_0 = 55\,\mathrm{mm\,s^{-1}}$, $h = 16\,\mathrm{mm}$, $\rho = 940\,\mathrm{kg\,m^{-3}}$, $\mu = 0.05\,\mathrm{Pa\,s}$ ($Re = 119$).

slow centrifugal flow, the small radial flow might have been responsible for the difference observed near the upper plate. In order to confirm this explanation, a second apparatus was built which avoided the problem of the centrifugal flow. This apparatus consisted of a straight channel enclosed in a Plexiglas box 2 m long, 0.066 m high and 0.120 m wide (figure 8). The wavy bottom was a bed of particles – no fixed bottom – deposited on a horizontal plate placed at mid-height in the box. The Couette flow was created by the oscillating motion of two plates, close to the upper and lower walls of the enclosing box. Both plates were driven by an electric motor monitored by a computer, through a system of pulleys and cables as sketched in figure 8. The upper plate created the shear flow above the bed, whereas the lower plate drove a backflow to avoid a longitudinal pressure gradient. The maximum allowed amplitude of the plate motion was $U_0/\omega = 200\,\mathrm{mm}$. The thickness h of the fluid layer was varied between 11 mm and 16 mm.

In order to verify that the upper and lower flows were balanced and that there was no residual pressure gradient, the bed of particles was replaced by a flat rigid plate, and fluid velocity was measured using a PIV technique, up to $Re = 119$. Figure 9 displays velocity profiles in the vertical plane of symmetry of the channel, at $Re = 119$

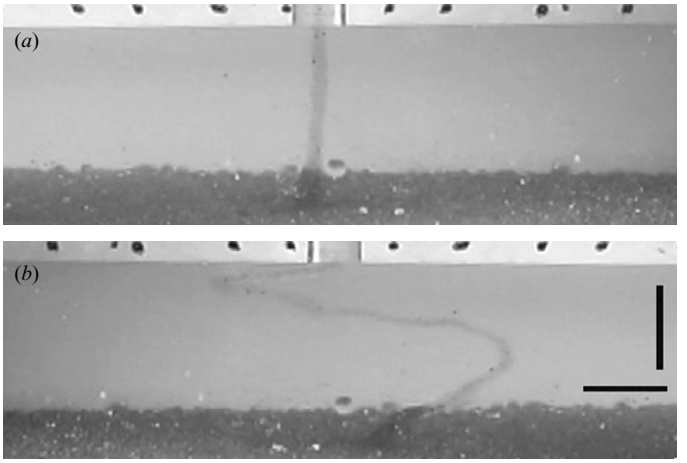

FIGURE 10. Dyed filament in the straight channel with the erodible bed, on the right side of a self-formed ripple: (*a*) initial straight filament; (*b*) deformed filament after eight periods of oscillation; the length of the dark marks is 5 mm. Parameters: $h = 0.011$ m, $\mu = 0.05$ Pa s, $U_0 = 0.07$ m s^{-1} and $f = 0.5$ Hz; $2\pi/k \approx 0.070$ m, $\eta_0 \approx 1.1$ mm ($k\eta_0 \approx 0.10$, $\epsilon \approx 0.1$, $Re = 7.1$ and $A = 2.0$).

and phases of the oscillation separated by $2\pi/5$. These measurements are compared to the expected parallel flow at the same Reynolds number, governed by the momentum equation $\rho\partial_t U = \mu\partial_{yy} U$ with the no-slip boundary conditions at the walls. It can be seen that the agreement between the measurements and the expected flow is quite good. Such a good agreement was found to hold in the middle half-width of the channel, as well as in its middle half-length (1 m). Note that the Reynolds number for all the subsequent experimental data is much smaller.

The vertical dyed filament was deposited in the channel as shown in figure 10(*a*). As the number of oscillations increases, the drift becomes apparent, with the filament remaining in the vertical plane: figure 10(*b*) corresponds to the flow over an erodible rippled bed after eight oscillations. As in the annular channel, the drift is directed towards the crest in the upper part of the fluid layer and towards the trough at mid-height, in agreement with the Lagrangian calculations. At a distance of about 1 mm above the bed, the displacement of the filament is small, so that its direction cannot be decided because the particles oscillate, and this motion mixes the fluid and blurs the filament.

Figure 11 compares the predictions to measurements over an erodible rippled bed. As for the annular channel, the small-amplitude calculation predicts larger velocity, whereas the large-amplitude calculation provides good agreement. When compared to figure 7, it can be seen that the agreement between measurements and calculations near the upper plate is better in the straight channel than in the annular channel, confirming our expectation about the effect of the slow centrifugal flow.

7. Conclusion

As discussed in the introduction, the usual explanation of ripple growth on an erodible bed is that the mean motion of particles from troughs to crests is driven by the mean fluid flow created by advection. Flow calculations assume that the bed is fixed and that the particle flux is related to the bed shear stress by some semi-empirical

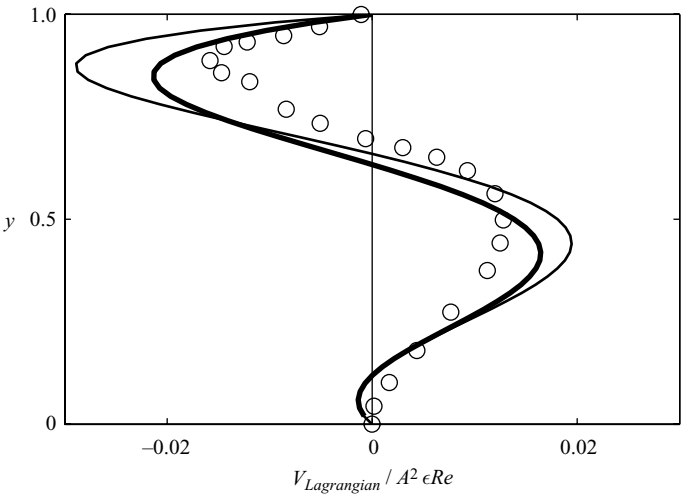

FIGURE 11. Observed drift of the dyed filament in the straight channel (○) compared to the calculations for $A \ll 1$ (thin curve) and $A = 2.0$ (thick curve). Same parameters as in figure 10.

power law similar to those used for steady flow. These assumptions, which ignore in particular the effect of particle motion on the fluid flow as well as particle inertia, have not received any experimental confirmation until now, with quantitative assessment. Hence the motivation of this paper, which reports quantitative measurements of the mean drift in viscous Couette flow, with comparison with theory; observations on particles motion are postponed to a future paper. The mean drift of a dyed filament of fluid was measured over artificial and self-formed ripples. In both cases this drift appears to be towards the crests near the upper part of the channel and away from the crests in the lower part, except very near the bed where it is oriented again towards the crests.

Since the fluid thickness was smaller than the thickness of any oscillating boundary layer and since the amplitude of the oscillations was not small, none of the available calculations was relevant, and new calculations were needed. The sense of the Eulerian drift was found to be opposite to that of the filament; however Lagrangian calculations allowed the right sense to be recovered. The small-amplitude Lagrangian drift, which is the sum of the Eulerian mean flow (3.1) and the Stokes drift (4.1), overpredicts the measured drift of the filament. Large-amplitude calculations (5.1) provide much better, quantitative, agreement. It was found that the Stokes drift dominates the Eulerian mean except very near the bottom boundary, where the Stokes drift vanishes quadratically and the Eulerian mean vanishes linearly. Thus the Lagrangian mean flow is towards the crests in a thin region next to the bottom boundary, of thickness 0.12 times that of the fluid layer. In the experiments, this thickness was about 1 mm which is larger than the particle diameter; however larger particles would be sensitive to reverse Lagrangian mean flow, down to troughs.

REFERENCES

BAGNOLD, R. 1946 Motion of waves in shallow water. interaction between waves and sand bottoms. *Proc. R. Soc. Lond.* A **187**, 1–18.

BATCHELOR, G. K. 1967 *An introduction to fluid dynamics*. Cambridge University Press.

Benjamin, T. B. 1959 Shearing flow over a wavy boundary. *J. Fluid Mech.* **6**, 161–205.

Blondeaux, P. 1990 Sand ripples under sea waves. Part 1. Ripple formation. *J. Fluid Mech.* **218**, 1–17.

Charru, F. 2006 Selection of the ripple length on a granular bed sheared by a liquid flow. *Phys. Fluids* **18**, 121508.

Charru, F. & Hinch, E. J. 2006*a* Ripple formation on a particle bed sheared by a viscous liquid. Part 1. Steady flow. *J. Fluid Mech.* **550**, 111–121.

Charru, F. & Hinch, E. J. 2006*b* Ripple formation on a particle bed sheared by a viscous liquid. Part 2. Oscillating flow. *J. Fluid Mech.* **550**, 123–137.

Charru, F., Larrieu, E., Dupont, J.-B. & Zenit, R. 2007 Motion of a particle near a rough wall in a viscous shear flow. *J. Fluid Mech.* **570**, 431–453.

Charru, F. & Mouilleron-Arnould, H. 2002 Instability of a bed of particles sheared by a viscous flow. *J. Fluid Mech.* **452**, 303–323.

Charru, F., Mouilleron-Arnould, H. & Eiff, O. 2004 Erosion and deposition of particles on a bed sheared by a viscous flow. *J. Fluid Mech.* **519**, 55–80.

Craik, A. D. D. 1982 The drift velocity of water waves. *J. Fluid Mech.* **116**, 187–205.

Du Toit, S. G., & Sleath, J. F. A. 1981 Velocity measurements close to rippled beds in oscillatory flow. *J. Fluid Mech.* **112**, 71–96.

Hara, T. & Mei, C. C. 1990 Oscillating flows over periodic ripples. *J. Fluid Mech.* **211**, 183–209.

Hara, T., Mei, C. C. & Shum, K. T. 1992 Oscillating flows over periodic ripples of finite slope. *Phys. Fluids* A **4**, 1373–1384.

Kaneko, A. & Honji, H. 1979 Double structures of steady streaming in the oscillatory viscous flow over a wavy wall. *J. Fluid Mech.* **93** (4), 727–736.

Lighthill, J. 1978 Acoustic streaming. *J. Sound Vib.* **61**, 391–418.

Longuet-Higgins, M. S. 1953 Mass transport in water waves. *Phil. Trans. R. Soc. Lond.* A **245**, 535–581.

Longuet-Higgins, M. S. 1981 Oscillating flow over steep sand ripples. *J. Fluid Mech.* **107**, 1–35.

Lyne, W. H. 1971 Unsteady viscous flow over a wavy wall. *J. Fluid Mech.* **50**, 33–48.

Marin, F. 2004 Eddy viscosity and Eulerian drift over rippled beds in waves. *Coastal Engng* **50**, 139–159.

Mei, C. C. & Yu, J. 1997 The instability of sand ripples under partially standing surface waves. *Phys. Fluids* **9**, 1609–1620.

Ourmières, Y. & Chaplin, J. R. 2004 Visualizations of the disturbed-laminar wave-induced flow above a rippled bed. *Exp. Fluids* **36**, 908–918.

Ourmières, Y. & Mouazé, D. 2007 Wave-induced boundary layer flows over a flat and rippled bed. *J. Hydraul. Res.* **45**, 239–253.

Rayleigh, L. 1883 On the circulation of air observed in Kundt's tubes and some allied acoustical problems. *Phil. Trans. R. Soc. Lond.* A **175**, 1–21.

Riley, N. 1965 Oscillating viscous flows. *Mathematika* **12**, 161–175.

Riley, N. 2001 Steady streaming. *Annu. Rev. Fluid Mech.* **33**, 43–65.

Rousseaux, G., Yoshikawa, H., Stegner, A. & Wesfreid, J. E. 2004 Dynamics of transient eddy above rolling-grain ripples. *Phys. Fluids* **16**, 1049–1058.

Scandura, P. 2007 Steady streaming in a turbulent oscillating boundary layer. *J. Fluid Mech.* **571**, 265–280.

Schaflinger, U., Acrivos, A. & Stibi, H. 1995 An experimental study of viscous resuspension in a pressure-driven plane channel flow. *Intl J. Multiphase Flow* **21**, 693–704.

Schlichting, H. 1932 Berechnung ebener periodischer Grenzschichtstrmungen *Phys. Z.* **33**, 327–335.

Shum, K. T. 1995 A numerical study of the wave-induced solute transport above a rippled bed. *J. Fluid Mech.* **299**, 267–288.

Sleath, J. F. A. 1974 Mass transport over a rough bed. *J. Mar. Sci.* **32**, 13–24.

Sleath, J. F. A. 1976 On rolling-grain ripples. *J. Hydraul. Res.* **14**, 69–81.

Stokes, G. G. 1847 On the theory of oscillatory waves. *Camb. Trans.* **8**, 441–473.

Stuart, J. T. 1963 Unsteady boundary layers. In *Laminary Boundary Layers* (ed. L. Rosenhead), pp. 349–408. Oxford University Press.

Unluata, U. & Mei, C. C. 1970 Mass transport in water waves *J. Geophys. Res.* **75**, 7611–7618.

Vittori, G. 1989 Non-linear viscous oscillatory flow over a wavy wall. *J. Hydraul. Res.* **27**, 267–280.

Vittori, G. & Blondeaux, P. 1990 Sand ripples under sea waves. Part 2. Finite-amplitude development. *J. Fluid Mech.* **218**, 19–39.

Wallner, J. & Schaflinger, U. 1998 Viscous resuspension of a sediment caused by oscillating stratified flows. *Acta Mech.* **127**, 147–153.

Zoueshtiagh, F., Thomas, P. J., Thomy, V. & Merlen, A. 2008 Micrometric granular ripple patterns in a capillary tube. *Phys. Rev. Lett.* **100**, 054501.